Eur. Phys. J. A **12**, 413–419 (2001)

THE EUROPEAN PHYSICAL JOURNAL A

Microscopic three-cluster study of the low-energy ^{9}Be photodisintegration

P. Descouvemont[a]

Physique Nucléaire Théorique et Physique Mathématique, Université Libre de Bruxelles, CP229, B-1050 Brussels, Belgium

Received: 7 September 2001 / Revised version: 25 October 2001
Communicated by P. Schuck

Abstract. The ^{9}Be and ^{9}B nuclei are investigated in a microscopic three-cluster model involving $\alpha+\alpha+n$ (or $\alpha+\alpha+p$) configurations. The $^8\mathrm{Be}(0^+,2^+)+n$ and $^5\mathrm{He}(3/2^-,1/2^-)+\alpha$ (or mirror) channels are included by taking account of the unstable nature of ^{8}Be and ^{5}He. Spectroscopic properties of ^{9}Be and ^{9}B are analyzed. We show that the $^5\,\mathrm{He}+\alpha$ configurations cannot be neglected to derive accurate results. The $^9\mathrm{Be}(\gamma,\alpha\alpha)n$ photodisintegration cross-section is shown to be mainly determined by $^8\mathrm{Be}+n$ channels at low energies, but $^5\,\mathrm{He}+\alpha$ channels become important beyond $E_\gamma\approx 4$ MeV.

PACS. 25.40.Lw Radiative capture – 24.50.+g Direct reactions – 25.60.Bx Elastic scattering

1 Introduction

Nucleosynthesis of heavy elements in exploding environments is expected to occur through the $\alpha(\alpha n,\gamma)^9$Be three-body reaction, followed by the $^9\mathrm{Be}(\alpha,n)^{12}$C reaction [1]. This sequence provides a bridge between $A=5$ and $A=8$ elements and proceeds more rapidly than the triple-α process. The cross-section for the former reaction is deduced from the $^9\mathrm{Be}+\gamma$ photodisintegration cross-section, which has been measured by several groups [2–7] and by different techniques. At low energies, the cross-section is believed to be essentially given by the properties of the $1/2^+$ resonance, located close to the $\alpha+\alpha+n$ threshold in ^{9}Be. In this energy regime, the $^8\mathrm{Be}+n$ breakup channel provides the main contribution, but the $^5\,\mathrm{He}+\alpha$ channel could be non-negligible at higher energies. In the theoretical point of view, an R-matrix analysis of the data has been performed by Barker [8], who determines the properties of the $1/2^+$ resonance through the cross-section data. On the other side, the theoretical investigation by Efros *et al.* [9] aims at fitting the data with a potential model in a limited energy range ($Q\leq E_\gamma\leq 2.2$ MeV), where Q is the particle threshold (1.66 MeV).

The spectroscopy of the ^{9}Be and ^{9}B mirror nuclei also presents many interesting aspects. The ^{9}Be nucleus is a so-called "Borromean" nucleus since it does not possess any bound two-body subsystem. As mentioned above, the existence of an s-wave neutron resonance near the threshold is responsible for peculiar properties [8]. On the other hand, it has been recently suggested [10] that Be isotopes, such as ^{9}Be, should present molecular states in their energy spectrum. Alpha clustering is well known in ^{7}Be and ^{8}Be, but is also expected to appear in excited states of other Be isotopes. Finally, the spectrum of the unbound ^{9}B nucleus still raises several interesting questions regarding the properties of its first excited states [11–13]. In addition, a recent experiment investigating the ^{9}C β-decay suggests the existence of narrow excited states in ^{9}B [14] which still needs a theoretical interpretation.

Many theoretical works have been devoted to the ^{9}Be and ^{9}B nuclei. We refer the reader to refs. [13,15] for recent references. Microscopic calculations involving $\alpha+\alpha+n$ configurations were first performed by Furutani *et al.* [16], and subsequently extended by improving the conditions of the calculations [17,15]. In ref. [15], Arai *et al.* use the stochastic variational method to optimize the $\alpha+\alpha+n$ basis. Although those authors could derive approximate widths of resonances through the Complex Rotation Method, their study is limited to spectroscopic properties. In the present work, we aim at analyzing the $^9\mathrm{Be}+\gamma$ photodisintegration cross-section in a microscopic model. To define the wave functions, we use the three-cluster model of ref. [17] improved in different ways: i) the ^{8}Be wave function is described more realistically, and ii) $^5\,\mathrm{He}+\alpha$ channels, missing in ref. [17], are taken into account here. As in ref. [17], the $^8\mathrm{Be}(2^+)+n$ configuration is included in the basis.

This microscopic multicluster model has been used in the past to investigate several light elements, especially exotic nuclei [18]. Starting from a nucleon-nucleon interaction and from some assumptions on the cluster structure, a microscopic model does not contain any further parameter and consequently presents a significant

[a] Directeur de Recherches FNRS; e-mail: pdesc@ulb.ac.be

predictive power. Our approach combines bound and scattering states of the nucleus. Using the microscopic R-matrix formalism [19] provides an exact account of boundary conditions. We are therefore able to study the ^{9}Be spectroscopy and the $^9\mathrm{Be}(\gamma,\alpha\alpha)n$ cross-section within the same conditions of calculation.

In sect. 2, we briefly present the model by emphasizing the properties of 9-nucleon systems. Section 3 is devoted to the spectroscopy of ^{9}Be and ^{9}B, and sect. 4 to the $^9\mathrm{Be}(\gamma,\alpha\alpha)n$ photodisintegration cross-section. Concluding remarks are presented in sect. 5.

2 The model

We use a microscopic model where the Hamiltonian involves space, spin and isospin coordinates of the nine nucleons. The effective nucleon-nucleon interaction is the Volkov $V2$ force [20] complemented by a zero-range spin-orbit term [21]. The parameters of the interaction (exchange parameter M for the central $V2$ force, and amplitude S_0 for the spin-orbit force) will be specified in the following.

To solve approximately the Schrödinger equation associated with the microscopic Hamiltonian, we apply the Generator Coordinate Method (GCM) to define the basis functions. A general presentation of the GCM can be found in ref. [18]; here we limit ourselves to the peculiarities of the ^{9}Be nucleus. In a three-cluster model involving two α-particles and a neutron, two coupling modes are possible: $^8\mathrm{Be}+n$ and $^5\mathrm{He}+\alpha$; these configurations will be hereafter denoted as 8-1 and 5-4, respectively. In a partial wave with total spin J and parity π, the wave function reads

$$\Psi^{JM\pi} = \Psi^{JM\pi}_{8\text{-}1} + \Psi^{JM\pi}_{5\text{-}4}, \tag{1}$$

where each term is defined, in the cluster approximation, as

$$\Psi^{JM\pi}_{8\text{-}1} = \sum_{I_1\ell I} \mathcal{A}\left[[\phi^{I_1}_8 \otimes \phi^{1/2}_1]^I \otimes Y_\ell(\hat{\boldsymbol{\rho}}_{8\text{-}1})\right]^{JM} \times g^{J\pi}_{4\text{-}8,I_1\ell I}(\rho_{8\text{-}1}) \tag{2}$$

and

$$\Psi^{JM\pi}_{5\text{-}4} = \sum_{I_1\ell} \mathcal{A}\phi^0_4\left[\phi^{I_1}_5 \otimes Y_\ell(\hat{\boldsymbol{\rho}}_{5\text{-}4})\right]^{JM} \times g^{J\pi}_{5\text{-}4,I_1\ell}(\rho_{5\text{-}4}), \tag{3}$$

where $\boldsymbol{\rho}$ represent the relative coordinates. Notice that wave functions (2) and (3) are not orthogonal to each other. In these definitions $\phi^{I_1}_8$, $\phi^{1/2}_1$, $\phi^{I_1}_5$ and ϕ^0_4 stand for the ^{8}Be, neutron, ^{5}He and α wave functions, respectively, $\mathcal{A}$ is the 9-body antisymmetrization operator, and $g^{J\pi}$ are the relative functions. In the three-cluster model, ^{8}Be and ^{5}He wave functions are themselves defined in the GCM as

$$\phi^{I_1K_1}_8 = \mathcal{A}\,\phi^0_4\,\phi^0_4\,Y^{K_1}_{I_1}(\hat{\boldsymbol{\rho}}_{4\text{-}4})\,g^{I_1}_{4\text{-}4}(\rho_{4\text{-}4})\,,$$
$$\phi^{I_1K_1}_5 = \mathcal{A}\phi^0_4\left[\phi^{1/2}_1 \otimes Y_\ell(\hat{\boldsymbol{\rho}}_{4\text{-}1})\right]^{I_1K_1} g^{I_1}_{4\text{-}1,\ell}(\rho_{4\text{-}1}). \tag{4}$$

Wave functions (2) and (3) are defined here with exact boundary conditions. This property is not necessary for spectroscopic properties [15] but it is required for scattering studies.

In the GCM, all radial wave functions g are expanded over a set of generator coordinates (R_1 for the $^8\mathrm{Be}+n$ and $^5\mathrm{He}+\alpha$ motion, and R_2 for the $\alpha+\alpha$ and $\alpha+n$ subsystems). We take 9 values for R_1 (from 1.2 fm to 10.8 fm with a step of 1.2 fm) and 4 values for R_2 (0.5 fm to 5.0 fm for ^{8}Be and 1 fm to 5.5 fm for ^{5}He). Using several R_2-values enables us to account for core deformation during the collision, and to simulate the unstable nature of ^{8}Be and ^{5}He. The present conditions of calculation represent an improvement with respect to ref. [17] since the ^{8}Be wave functions are described here with a larger set of generator coordinates, yielding a more realistic structure; on the other hand, the $^5\mathrm{He}+\alpha$ channel, open at fairly low energies, was not considered in ref. [17].

In eqs. (2)-(4), I_1 denotes the spin of ^{8}Be and of ^{5}He; the 0^+ and 2^+ states of ^{8}Be are included, as well as the $3/2^-$ and $1/2^-$ partial waves of ^{5}He. The use of the GCM enables us to write down the total wave functions appearing in eq. (1) as

$$\Psi^{JM\pi}_i = \sum_{I_1\ell I}\sum_{R_1,R_2} f^{J\pi}_{i,I_1\ell I}(R_1,R_2)\,\Phi^{JM\pi}_{i,I_1\ell I}(R_1,R_2), \tag{5}$$

where i represents the 8-1 or 5-4 configurations, $\Phi^{JM\pi}_i$ are projected Slater determinants and $f^{J\pi}$ the generator functions. Definitions (2)-(3) and (5) are known to be quite equivalent, but the use of Slater determinants is well adapted to numerical calculations.

The first step is to compute matrix elements of the Hamiltonian between projected Slater determinants $\Phi^{JM\pi}$. Then, we use the microscopic R-matrix formalism to derive the generator functions, and the asymptotic behavior of the wave functions. Capture cross-sections also require the calculation of matrix elements of the electromagnetic multipole operators. We refer the reader to refs. [22,18] for detail concerning the technical procedure.

3 Spectroscopic properties of ^{9}Be and ^{9}B

3.1 Conditions of the calculation

The oscillator parameter is taken as $b = 1.36$ fm, which minimizes the α binding energy. The spin-orbit amplitude is chosen as $S_0 = 30$ MeV fm^5, a typical value for p-shell nuclei. For the Majorana parameter we have adopted $M = 0.593$ which reproduces the $1/2^+$ resonance energy in the $^9\mathrm{Be}(\gamma,\alpha\alpha)n$ experimental cross-section. This choice is fairly close to the standard value $M = 0.6$.

With these conditions, we have computed the energy curves given in fig. 1. The energy curves [18] represent the expectation energy of the system for a fixed value of the generator coordinate R_1 (diagonalization is performed over partial waves $I_1\ell I$ and generator coordinate R_2). They provide a useful information regarding the physics of the system. A first conclusion is that, except for the $1/2^+$

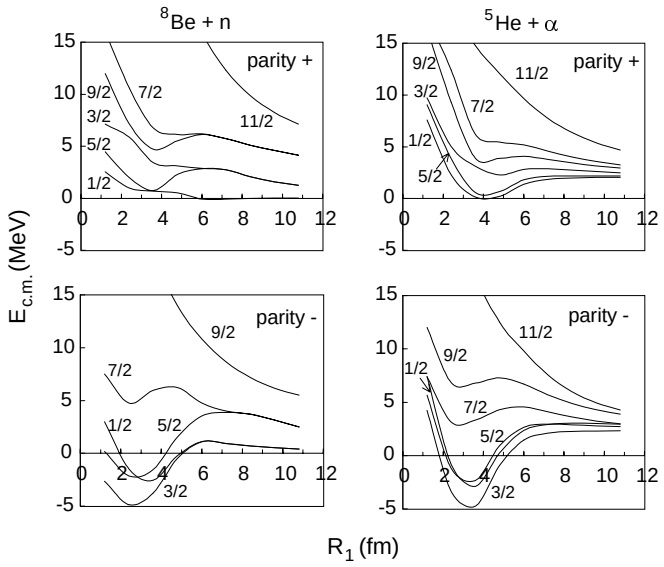

Fig. 1. $^8\mathrm{Be}+n$ and $^5\mathrm{He}+\alpha$ energy curves. The zero energy is defined at the $^8\mathrm{Be}+n$ threshold.

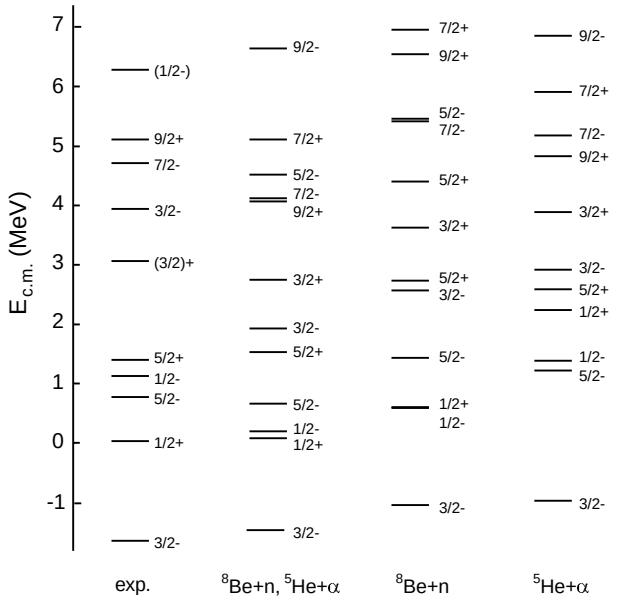

Fig. 2. ^{9}Be spectrum with different configurations. The data are taken from refs. [23,24].

partial wave, the $^8\mathrm{Be}+n$ and $^5\mathrm{He}+\alpha$ energy curves are rather similar to each other. This is not surprising in a microscopic model where, at short distances, the antisymmetrization makes all nucleons equivalent and reduces the cluster structure of the nucleus. As expected, the lowest minimum is found in the $3/2^-$ partial wave which corresponds to the ^{9}Be ground state. In positive parity, minima are obtained up to $J = 9/2$. In negative parity, high partial waves ($7/2^-$ and $9/2^-$) present lower energies in the $^5\mathrm{He}+\alpha$ channel. This configuration should therefore play a major role in high-spin states.

3.2 The ^{9}Be nucleus

The ^{9}Be spectrum is presented in fig. 2 with 3 different conditions of calculation: single channel $^8\mathrm{Be}+n$ or $^5\mathrm{He}+\alpha$, and the multichannel approach. Energies are given with respect to the $^8\mathrm{Be}+n$ threshold. Let us recall that the nucleon-nucleon interaction has been adjusted on the experimental energy of the $1/2^+$ state. This choice yields also a fairly good binding energy for the $3/2^-$ ground state. The simultaneous description of positive-parity and negative-parity states represents an improvement with respect to the previous calculation [17] where a significant parity effect had to be introduced in the nucleon-nucleon force.

The $3/2^-$ ground-state energy is nearly independent of the configuration; this result supports low clustering effects. On the contrary, the $1/2^+$ state, located very close to the neutron threshold, is better reproduced (by about 2 MeV) with the $^8\mathrm{Be}+n$ configuration. This conclusion is consistent with the energy curves of fig. 1 which show that the $^8\mathrm{Be}+n$ channel dominates in the $1/2^+$ partial wave. The multichannel calculation reproduces fairly well the experimental states up to $E_{\mathrm{c.m.}} \approx 5$ MeV, but the $1/2^-$ and $3/2^-_2$ resonances are slightly overbound by the GCM. This

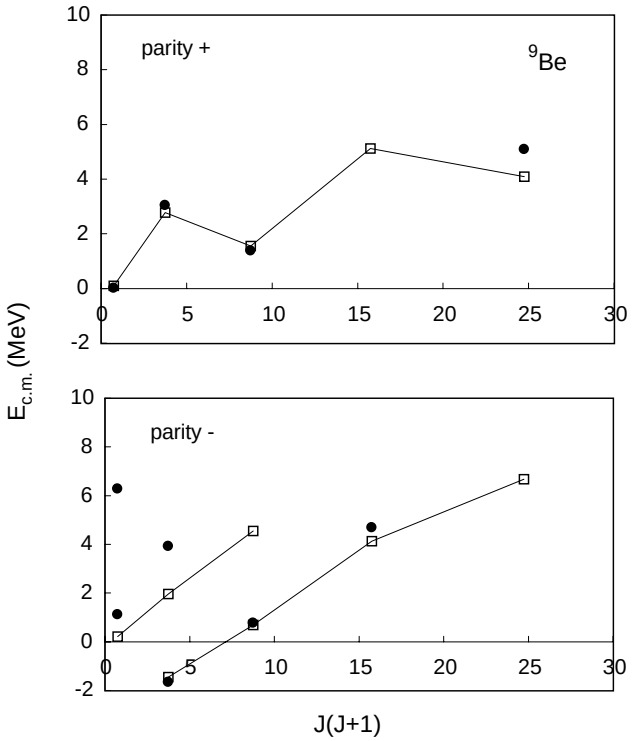

Fig. 3. Band structure of ^{9}Be. Squares represent the GCM results, and circles the experimental data of refs. [23,24].

overbinding was also present in the microscopic calculation of Arai *et al.* [15] for the $3/2^-_2$ state. For high-spin states ($J \geq 7/2$), the $^5\mathrm{He}+\alpha$ configuration gives lower excitation energies, in agreement with the energy curves of fig. 1.

The band structure is presented in fig. 3. In positive parity, the spin-orbit force makes states with $J = \ell - 1/2$

Table 1. Energies (in MeV, and with respect to the $^8\mathrm{Be}+n$ threshold), total widths (in MeV), and dimensionless reduced widths (in %, calculated at 10.8 fm).

State	$E_{\mathrm{c.m.}}$	Γ	θ_0^2	θ_2^2	θ_α^2
$1/2^+$	0.10	0.36	43.3	0.049	0.2
$3/2^+$	2.77	0.47	12.9	7.7	4.1
$5/2^+$	1.56	0.25	11.3	0.9	1.6
$7/2^+$	5.12	1.20	0.1	16.0	35.0
$9/2^+$	4.09	0.52	0.1	8.9	31.1
$3/2^-$	-1.45		0.9	0.041	0.020
$5/2^-$	0.88	1.57×10^{-5}	0.0046	0.9	0.2
$7/2^-$	4.26	1.07	1.6	24.7	21.0
$9/2^-$	6.67	2.32	0.0032	0.8	87.5
$1/2^-$	0.21	0.09	13.9	0.2	0.019
$3/2^-$	1.96	0.26	7.5	1.9	0.2
$5/2^-$	4.57	1.63	0.5	7.5	69.4

Table 2. $E1$ and $E2$ transition probabilities in ^{9}Be (in Wu).

Transition	GCM	Experiment [23]
$1/2^+ \to 3/2^-_1$	0.40	$0.22\pm0.09, 0.38\pm0.03$ [7]
$5/2^+ \to 3/2^-_1$	0.15	0.14 ± 0.01 [7]
$3/2^+ \to 3/2^-_1$	0.05	
$5/2^-_1 \to 3/2^-_1$	29.1	24.4 ± 1.8
$7/2^-_1 \to 5/2^-_1$	16.4	
$7/2^-_1 \to 3/2^-_1$	13.3	6.3 ± 2.7
$9/2^-_1 \to 7/2^-_1$	54.7	
$9/2^-_1 \to 5/2^-_1$	16.1	
$3/2^-_2 \to 1/2^-_1$	17.8	
$5/2^-_2 \to 1/2^-_1$	5.3	
$5/2^-_2 \to 3/2^-_2$	0.26	

higher than states with $J = \ell + 1/2$. A similar band structure is obtained in the molecular-orbit model of von Oertzen [10]. We predict a $7/2^+$ state which should be located near $E_x = 6.5$ MeV with a width of 1.2 MeV. In negative parity, we confirm the $3/2^-$ band built on the ground state. A $1/2^-$ band is predicted with the $1/2^-_1$ state as band head. The GCM overestimates the binding energies but the existence of a $5/2^-_2$ state near $E_x = 8$ MeV should be reliable. The experimental $1/2^-_2$ state near $E_{\mathrm{c.m.}} = 6$ MeV cannot be reproduced by an $\alpha+\alpha+n$ cluster model [15], which suggests that this state should have an isospin $T = 3/2$.

Table 1 presents spectroscopic properties of the ^{9}Be states. Dimensionless reduced widths, calculated at 10.8 fm, are given for the $^8\mathrm{Be}(0^+)+n$, $^8\mathrm{Be}(2^+)+n$ and $^5\mathrm{He}(3/2^-)+\alpha$ channels. The fit of the low-energy photodisintegration cross-section (see sect. 5) provides $E_{\mathrm{c.m.}} = 0.10$ MeV. This value is much lower than the width, which makes the energy partly model dependent. This problem has been already addressed by Barker [25]. In the $1/2^+$ band, we find an evolution of the structure, from an almost pure $^8\mathrm{Be}(0^+)+n$ configuration for $J = 1/2^+$, to a pronounced $^5\mathrm{He}(3/2^-)+\alpha$ structure for $J \geq 7/2^+$. This shows that the $1/2^+$ band cannot be rigorously considered as a $^8\mathrm{Be}(0^+)+n$ rotational band. For $J \geq 7/2^+$, the $^8\mathrm{Be}(2^+)+n$ channel also plays a significant role. The situation is similar in the $3/2^-$ band; low-lying states present a compact structure, characterized by small reduced widths. Clustering effects increase for higher J-values.

In table 2, we give $E1$ and $E2$ electromagnetic transition probabilities, compared with available experimental data [7]. No effective charge is used. The $B(E1)$ value for the $1/2^+ \to 3/2^-_1$ transition is in nice agreement with the recent value of Utsunomiya *et al.* [7]. Barker [8] has shown that the unbound nature of the $1/2^+$ state must be taken into account for a reliable calculation of the $B(E1)$-value. We obtain here a significant reduction compared with the previous microscopic calculation [17] (0.68 Wu); again this property emphasizes the importance of different clustering modes in ^{9}Be. The same conclusion holds for the $5/2^+ \to 3/2^-_1$ transition, for which the GCM nicely reproduces the experimental value. Calculation without the $^5\mathrm{He}+\alpha$ channel [17] yields $B(E1) = 0.32$ Wu which overestimates experiment by a factor of two. For $E2$ transition probabilities, little experimental information is available.

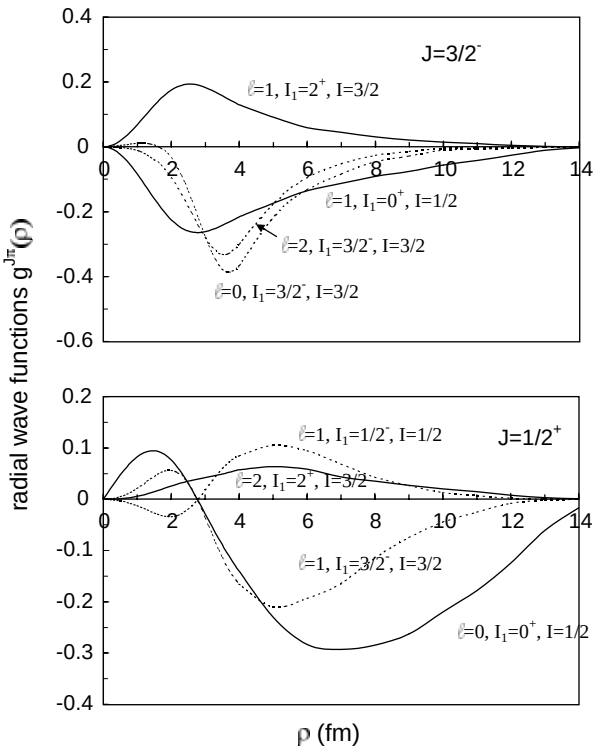

Fig. 4. ^{9}Be radial wave functions $g^{J\pi}$. The full curves correspond to $^8\mathrm{Be}+n$ channels, and the dotted curves to $^5\mathrm{He}+\alpha$ channels.

The quadrupole moment $Q = 5.7\ e\,\mathrm{fm}^2$ is consistent with experiment $Q = 5.3 \pm 0.3\ e\,\mathrm{fm}^2$ [23]. We also get a slight overestimation of the $5/2^-_1 \to 3/2^-_1$ transition probability. For the $7/2^-_1 \to 3/2^-_1$ transition, the difference reaches a factor of 2.

In fig. 4, we display some components of the $3/2^-$ and $1/2^+$ radial wave functions. Orthogonalization to the forbidden states has been performed according to the method presented in ref. [26]. For the ground state, the $^8\mathrm{Be} + n$ component ($\ell = 1$) extends much further than the other components since the binding energy is the lowest in this channel. The $^5\mathrm{He} + \alpha$ components are negligible at large distances but present a rather pronounced peak in the inner region, near 4 fm. The $1/2^+$ state is unbound and therefore its wave function presents an oscillating asymptotic behaviour. The $^8\mathrm{Be}(0^+) + n$ and $^5\mathrm{He}(3/2^-) + \alpha$ components present a node near 3 fm. As for the ground state, the $^8\mathrm{Be}(0^+) + n$ configuration is dominant, but other channels are not negligible.

3.3 The ^{9}B nucleus

The ^{9}B nucleus is studied with the mirror configurations of ^{9}Be, *i.e.* with $^8\mathrm{Be}(0^+, 2^+) + p$ and $^5\mathrm{Li}(3/2^-, 1/2^-) + \alpha$ cluster structures. Figure 5 presents the ^{9}B spectrum obtained with the same nucleon-nucleon force; nothing has been fitted on the ^{9}B nucleus. For this reason, slight inaccuracies on the energies may affect the widths. Several recent studies have been devoted to the ^{9}B nucleus [27, 13], especially to the $1/2^+$ first excited state. Barker [13] showed recently that the large width of this level prevents from an accurate determination of its energy. Properties of such a broad resonance are always, at least partially, model dependent. In ^{9}Be, the $1/2^+$ band is very well described by the GCM. This suggests to assign the experimental level at $E_x = 2.79$ MeV, whose spin is $3/2^+$ or $5/2^+$ to $J = 5/2^+$. The energy and width of the $5/2^+$ GCM state are in nice agreement with experimental properties of this state. The broad level at $E_x = 4.8$ MeV might be assigned to $J = 3/2^+$.

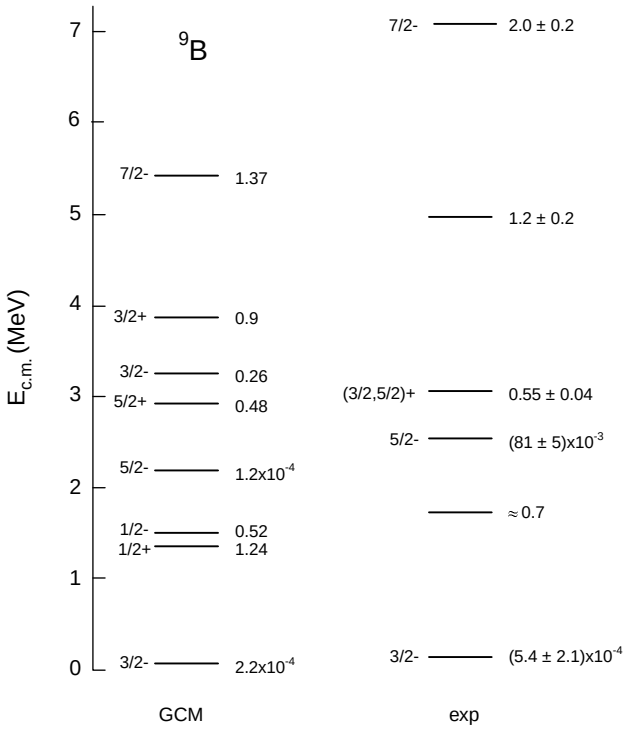

Fig. 5. ^{9}B spectrum. Energies are given with respect to the $^8\mathrm{Be} + p$ threshold. The widths (in MeV) are given at the right side of the energy levels.

Table 3. Energies (in MeV, and with respect to the $^8\mathrm{Be} + p$ threshold), total widths (in MeV), and dimensionless reduced widths (in %, calculated at 10.8 fm).

State	$E_{\mathrm{c.m.}}$	Γ	θ_0^2	θ_2^2	θ_α^2
$1/2^+$	1.41	1.24	48.2	0.050	0.2
$3/2^+$	3.94	0.90	11.2	22.9	2.6
$5/2^+$	2.98	0.48	14.6	0.10	2.0
$7/2^+$	6.4	1.5	0.2	20.6	35.0
$9/2^+$	5.4	0.8	0.2	12.9	32.0
$3/2^-$	0.14	2.2×10^{-4}	3.1	0.064	0.030
$5/2^-$	2.25	1.2×10^{-4}	0.0082	0.23	0.20
$7/2^-$	5.5	1.4	1.8	27.8	18.7
$9/2^-$	7.9	2.4	~ 0	0.7	87.3
$1/2^-$	1.57	0.52	21.8	0.3	0.020
$3/2^-$	3.31	0.26	6.0	7.9	0.2
$5/2^-$	5.9	1.8	0.5	7.2	69.2

Table 3 gives energies, total widths and dimensionless reduced widths of ^{9}B states. As for ^{9}Be, a band classification can be done, and a similar evolution of the structure is obtained. In general, charge symmetry is well reproduced; mirror states present similar reduced widths. For low-spin states, we find a dominant $^8\mathrm{Be}(0^+) + p$ configuration whereas the $^5\mathrm{Li}(3/2^-) + \alpha$ structure is more important for higher J-values. Clustering effects increase with J.

This work was partly motivated by the recent experiment of Gete *et al.* [14] who investigated the β-delayed particle decay of ^{9}C, and observed new ^{9}B states beyond $E_x = 10$ MeV. One of them ($E_x = 12.16$ MeV) is a $3/2^-$ state with a significant branching ratio to the $^5\mathrm{Li} + \alpha$ channel, indicating a $^5\mathrm{Li} + \alpha$ dominant cluster structure. The present GCM study does not give rise to such narrow excited states. The basis is fairly extended with several $\alpha + \alpha + p$ coupling modes, each of them being described with several generator coordinates. It seems reasonable to assume that this basis should reproduce all $T = 1/2$ narrow states. It is therefore likely that the highly excited states observed by Gete *et al.* correspond to $T = 3/2$ levels.

4 Photodisintegration of ^{9}Be

The dissociation of ^{9}Be may proceed in two ways: $^8\mathrm{Be} + n$, followed by the ^{8}Be breakup into $\alpha + \alpha$, and $^5\mathrm{He} + \alpha$,

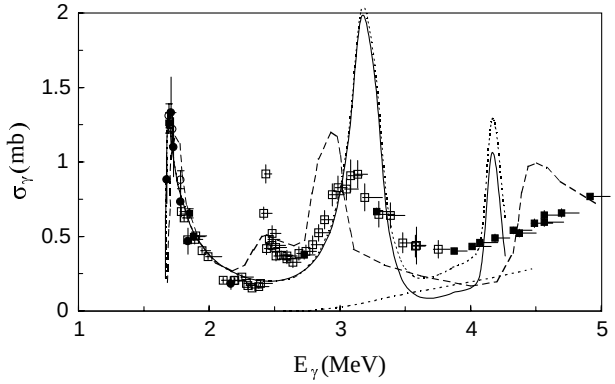

Fig. 6. Photodisintegration cross-section of ^{9}Be (full curve). The partial cross-sections to the $^8\mathrm{Be}+n$ and $^5\mathrm{He}+\alpha$ channels are shown as dotted lines. The experimental data are taken from ref. [4] (open circles), [5] (full circles), [7] (open squares: polarized data, full squares: non-polarized data) and [3] (long dashed curve).

followed by the ^{5}He breakup into $\alpha + n$. Although the second process is generally believed to be negligible, its influence has not been analyzed yet theoretically.

For a multipole of order λ, the photodisintegration cross-section to partial wave $J\pi$ of a channel i ($^8\mathrm{Be}+n$ or $^5\mathrm{He}+\alpha$) reads

$$\sigma_i^J(E_\gamma) = \frac{8\pi(\lambda+1)}{\hbar\lambda(2\lambda+1)!!2} k^2 k_\gamma^{2\lambda-1} \times \sum_{\ell I} \frac{4}{(2\ell+1)(2I+1)} |\langle \Psi(^9\mathrm{Be}) || \mathcal{M}_\lambda || \Psi_{i\ell I}^{J\pi}(E) \rangle|^2, \quad (6)$$

where E is the c.m. energy, E_γ the photon energy and $\mathcal{M}_\lambda$ the electromagnetic multipole operator (we take here the $E1$ term only). In eq. (6), $\Psi_{il I}^{J\pi}(E)$ is a partial wave of a unit-flux scattering function [22]. The total photodisintegration cross-section is obtained by summing over channels and spins

$$\sigma(E_\gamma) = \sum_{i,J} \sigma_i^J(E_\gamma). \quad (7)$$

The GCM cross-section is presented in fig. 6 and compared with available experimental data. These data have been obtained by using different techniques: bremsstrahlung [3, 6], radioactive isotopes [2,4,5] and polarized or unpolarized photon beams [7]. They are not inconsistent with each other, but some differences are not negligible.

Near the threshold, the cross-section is essentially determined by the properties of the $1/2^+$ resonance. The Majorana parameter, involved in the Volkov nucleon-nucleon interaction, was chosen in order to reproduce as well as possible the data just above the threshold. Since the $M1$ multipolarity is not included in the multipole expansion, the $5/2^-$ resonance at $E_\gamma = 2.49$ MeV does not show up in the GCM curve. Around $E_\gamma = 3$ MeV, the broad peak corresponds to the $5/2^+$ resonance, whose energy is well predicted by the model (see fig. 2). As shown in table 2, the GCM γ width agrees fairly well with experiment, but the theoretical neutron width is slightly too small. The GCM curve shows a $3/2^+$ resonance (see fig. 2) near $E_\gamma = 4$ MeV; this is consistent with the maximum observed in the data of Jakobson [3], although the theoretical energy is slightly lower. The recent data of Utsunomiya *et al.* [7], however, do not support the existence of a $3/2^+$ resonance.

Below $E_\gamma = 3$ MeV, fig. 6 indicates that the $^8\mathrm{Be}+n$ breakup channel is the main contribution to the photodisintegration cross-section. The $^5\mathrm{He}+\alpha$ channel becomes more and more important as the energy increases, but the partial cross-section is essentially non-resonant. This is consistent with the reduced widths given in table 1; reduced α widths of the $3/2^+$ and $5/2^+$ resonances are lower than the reduced neutron widths, and the higher threshold of the $^5\mathrm{He}+\alpha$ channel still reduces its contribution.

5 Conclusion

In this paper, we have analyzed the ^{9}Be and ^{9}B mirror nuclei, and the $^9\mathrm{Be}+\gamma \rightarrow n+\alpha+\alpha$ photodisintegration cross-section simultaneously. The nucleon-nucleon interaction is kept identical for each calculation. The basis wave functions are built in a three-cluster microscopic model, with exact boundary conditions. This is necessary to investigate scattering states. For ^{9}Be, two arrangements of the $\alpha+\alpha+n$ clusters have been considered: $^8\mathrm{Be}(=\alpha+\alpha)+n$ and $^5\mathrm{He}(=\alpha+n)+\alpha$; the mirror channels are taken into account for ^{9}B. In each case, excited states have been included, and special attention has been paid to distortion effects. The spectroscopy of ^{9}Be indicates that, when the spin increases, the $^5\mathrm{He}+\alpha$ component is more and more important. The necessity of including this channel also appears in the $B(E1)$-values between low-lying states, which are significantly overestimated if it is missing. The inclusion of $^5\mathrm{He}+\alpha$ channels yields rather precise energies for the $3/2^-$ and $1/2^+$ states simultaneously; neglecting these channels requires to use different nucleon-nucleon forces for negative- and positive-parity states [17]. We confirm the band structure suggested by von Oertzen [10], but the states evolve from a $^8\mathrm{Be}+n$ to $^5\mathrm{He}+\alpha$ cluster configuration.

The analysis of ^{9}B has been done without parameter adjustment. The ground-state energy is well reproduced. The $1/2^+$ excited state is very broad and a detailed comparison between theory and experiment is difficult [13]. The narrow states observed by Gete *et al.* [14] beyond $E_x = 13$ MeV could not be reproduced by the model, suggesting a $T = 3/2$ assignment for these states.

The GCM study of the ^{9}Be photodissociation cross-section is supported by the experimental data, but the precision of the model, which does not contain parameters when the interaction is fixed, is not high enough to disentangle the slight difference between the many data. However, the importance of the $^5\mathrm{He}+\alpha$ breakup, followed by the ^{5}He decay to $\alpha + n$, is clearly apparent beyond $E_\gamma = 4$ MeV.

I am grateful to Prof. D. Measday for discussions about the ^{9}B spectrum. This text presents research results of the Belgian program P4/18 on interuniversity attraction poles initiated by the Belgian-state Federal Services for Scientific, Technical and Cultural Affairs. This work is supported by the National Fund for Scientific Research (FNRS), Belgium.

References

1. S.E. Woosley, R.D. Hoffman, Astrophys. J. **395**, 202 (1992).
2. J.H. Gibbons, R.L. Macklin, J.B. Marion, H.W. Schmitt, Phys. Rev. **114**, 1319 (1959).
3. M.K. Jakobson, Phys. Rev. **123**, 229 (1961).
4. W. John, J.M. Prosser, Phys. Rev **127**, 231 (1962).
5. M. Fujishiro, T. Tabata, K. Okamoto, T. Tsujimoto, Can. J. Phys. **60**, 1672 (1982); M. Fujishiro, K. Okamoto, T. Tsujimoto, Can. J. Phys. **61**, 1579 (1983).
6. A.M. Goryachev, G.N. Zalesny, I.V. Pozdnev, Izv. RAN, Ser. Fiz. **56**, 159 (1992).
7. H. Utsunomiya, Y. Yonezawa, H. Akimune, T. Yamagata, M. Ohta, M. Fujishiro, H. Toyokawa, H. Ohgaki, Phys. Rev. C **63**, 018801 (2001).
8. F.C. Barker, Aust. J. Phys. **37**, 267 (1984).
9. V.D. Efros, H. Oberhummer, A. Pushkin, I.J. Thompson, Eur. Phys. J. A **1**, 447 (1998).
10. W. von Oertzen, Z. Phys. A **357**, 355 (1997).
11. M.A. Tiede, K.W. Kemper, N.R. Fletcher, D. Robson, D.D. Caussyn, S.J. Bennett, J.D. Brown, W.N. Catford, C.D. Jones, D.L. Watson, W.D.M. Rae, Phys. Rev. C **52**, 1315 (1995).
12. H.T. Fortune, Phys. Rev. C **52**, 2261 (1995).
13. F.C. Barker, Phys. Rev. C **53**, 2539 (1996).
14. E. Gete, L. Buchmann, R.E. Azuma, D. Anthony, N. Bateman, J.C. Chow, J.M. D'Auria, M. Dombsky, U. Giesen, C. Iliadis, K.P. Jackson, J.D. King, D.F. Measday, A.C. Morton, Phys. Rev. C **61**, 064310 (2000).
15. K. Arai, Y. Ogawa, Y. Suzuki, K. Varga, Phys. Rev. C **54**, 132 (1996).
16. H. Furutani, H. Kanada, T. Kaneko, S. Nagata, H. Nishioka, S. Okabe, S. Saito, T. Sakuda, M. Seya, Progr. Theor. Phys. Suppl. **68**, 193 (1980).
17. P. Descouvemont, Phys. Rev. C **39**, 1557 (1989).
18. P. Descouvemont, *Proceedings of the International Conference on Innovative Computational Methods in Nuclear Many-body Problems*, Osaka, Japan, edited by H. Horiuchi *et al.* (World Scientific, 1998) p. 205.
19. D. Baye, P.-H. Heenen, M. Libert-Heinemann, Nucl. Phys. A **291**, 230 (1977).
20. A.B. Volkov, Nucl. Phys. **74**, 33 (1965).
21. D. Baye, N. Pecher, Bull. Cl. Sc. Acad. Roy. Belg. **67**, 835 (1981).
22. D. Baye, P. Descouvemont, Nucl. Phys. A **407**, 77 (1983).
23. F. Ajzenberg-Selove, Nucl. Phys. A **490**, 1 (1988).
24. S. Dixit, W. Bertozzi, T.N. Buti, J.M. Finn, F.W. Hersman, C.E. Hyde-Wright, M.V. Hynes, M.A. Kovash, B.E. Norum, J.J. Kelly, A.D. Bacher, G.T. Emery, C.C. Foster, W.P. Jones, D.W. Miller, B.L. Berman, D.J. Millener, Phys. Rev. C **43**, 1758 (1991); J.P. Glickman, W. Bertozzi, T.N. Buti, S. Dixit, F.W. Hersman, C.E. Hyde-Wright, M.V. Hynes, R.W. Lourie, B.E. Norum, J.J. Kelly, B.L. Berman, D.J. Millener, Phys. Rev. C **43**, 1740 (1991).
25. F.C. Barker, Can. J. Phys. **61**, 1371 (1983).
26. M. Dufour, P. Descouvemont, Phys. Rev. C **56**, 1831 (1997).
27. F.C. Barker, Aust. J. Phys. **40**, 307 (1987).